

Prompt-Guided Adaptive Model Transformation for Whole Slide Image Classification

Yi Lin^{†1}, Zhengjie Zhu^{†1,2}, Kwang-Ting Cheng¹, and Hao Chen^{✉1}

¹ The Hong Kong University of Science and Technology, Hong Kong, China.

² The Hong Kong University of Science and Technology (Guangzhou), China.
jhc@cse.ust.hk

Abstract. Multiple instance learning (MIL) has emerged as a popular method for classifying histopathology whole slide images (WSIs). Existing approaches typically rely on frozen pre-trained models to extract instance features, neglecting the substantial domain shift between pre-training natural and histopathological images. To address this issue, we propose *PAMT*, a novel Prompt-guided Adaptive Model Transformation framework that enhances MIL classification performance by seamlessly adapting pre-trained models to the specific characteristics of histopathology data. To capture the intricate histopathology distribution, we introduce Representative Patch Sampling (RPS) and Prototypical Visual Prompt (PVP) to reform the input data, building a compact while informative representation. Furthermore, to narrow the domain gap, we introduce Adaptive Model Transformation (AMT) that integrates adapter blocks within the feature extraction pipeline, enabling the pre-trained models to learn domain-specific features. We rigorously evaluate our approach on two publicly available datasets, Camelyon16 and TCGA-NSCLC, showcasing substantial improvements across various MIL models. Our findings affirm the potential of *PAMT* to set a new benchmark in WSI classification, underscoring the value of a targeted reprogramming approach.

Keywords: Prompt learning; Multiple instance learning; Whole slide image; Parameter-efficient fine-tuning.

1 Introduction

Whole slide image (WSI) is indispensable in modern histopathology, offering a detailed view crucial for accurate clinical disease diagnosis and research [5,16,19]. The advent of deep learning techniques has significantly transformed histopathology image analysis, promising improvements in both precision and efficiency [6,17]. Despite these advancements, deep-learning-based WSI classification presents notable challenges due to the massive size of WSIs, necessitating the division of WSIs into smaller patches for analysis [8]. This patch-based approach, however,

[†] Equal contribution; ✉ corresponding author.

introduces labor-intensive and time-consuming annotation processes, limiting the effectiveness of supervised learning methods in this context [11,13].

To circumvent these limitations, multiple instance learning (MIL) has become the preferred strategy for WSI analysis. In MIL, a WSI is treated as a bag of patches, and the entire bag is labeled based on the presence or absence of disease indicators among its constituent patches. However, this method requires effective downsampling and feature extraction strategies to manage the voluminous data, with the quality of patch features directly impacting MIL classification outcomes [9,12,22,15]. Existing MIL-based methods mainly leverage pre-trained feature extractors without fine-tuning due to the unaffordable computational cost of training the entire model on the large-scale WSI datasets [9,12,22,15], ignoring the domain shift and task discrepancies between the pre-training task (*e.g.*, ImageNet) and the downstream task (*e.g.*, histopathology) [20]. To narrow the domain shift, researchers [12] propose to utilize self-supervised techniques such as SimCLR [4] to pre-train the feature extractor on pathology images. However, these methods fail to utilize available WSI labels, offering limited performance improvements. Recent advancements in parameter-efficient fine-tuning (PEFT), such as visual prompts [23] and adapter tuning [24], have shown promise in addressing domain shift and task discrepancies. However, the application of PEFT techniques in the context of WSI classification remains largely unexplored.

In this work, we propose *PAMT*, a Prompt-guided Adaptive Model Transformation framework that enhances WSI classification by ingeniously reprogramming both the input bags and intermediate features with the visual prompt and model adapter. To the best of our knowledge, this is the first attempt to adopt PEFT techniques in consideration of the unique and complex nature of pathological images. For this purpose, we first introduce Representative Patch Sampling (RPS) strategy to capture the most relevant and informative patches while discarding redundant ones, which extensively reduces the computational cost and enables efficient end-to-end training. Additionally, to encapsulate the diverse spectrum of pathological data distributions, we further propose Prototypical Visual Prompt (PVP) module, where visual prompts are added to the sampled patches, enhancing the model’s ability to interpret the wide array of tissue characteristics inherent to WSI. To facilitate model adaption, we introduce Adaptive Model Transformation (AMT) technique to modify the pre-trained feature extractor with scaleable adapters, allowing nuanced adaptation of ImageNet-trained architectures to the requirements of pathological image analysis. The pre-trained model is frozen while training visual prompts, adapter blocks, and a lightweight MIL classifier, ensuring the intrinsic knowledge of the model is maintained.

Our contributions are succinctly summarized as follows:

- We pioneer the application of parameter-efficient fine-tuning in the WSI classification domain, demonstrating the effectiveness of the PAMT framework in enhancing model adaptability and performance on pathological images.
- We propose Representative Patch Sampling (RPS) strategy, which efficiently distills informative patches from WSIs, enabling focused training on focus-

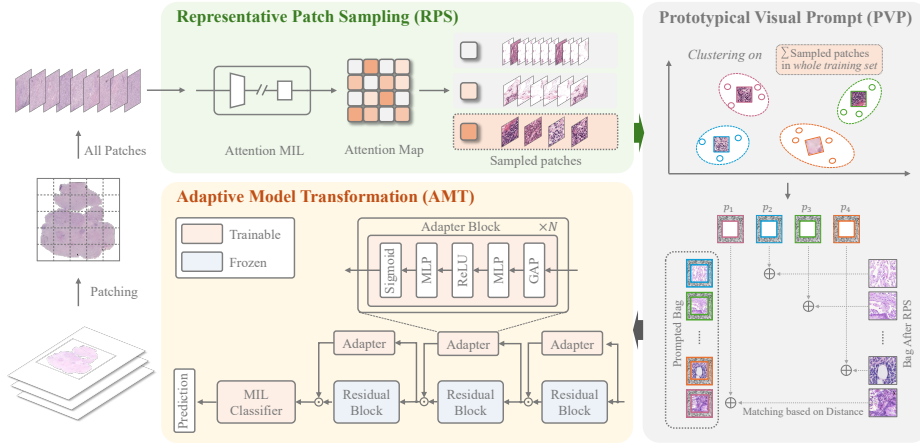


Fig. 1. Overview of the proposed method.

ing on diagnostically significant data and enhancing the model’s learning efficiency with an end-to-end training.

- We propose Prototypical Visual Prompt (PVP) module, which introduces visual prompts assigned by cluster centers to effectively capture the complex distribution of pathological features across varied histopathological images.
- We propose Adaptive Model Transformation (AMT) technique, which injects scaleable adapters into pre-trained feature extractor, facilitating a nuanced and efficient knowledge transformation from natural to pathological domain.
- Extensive experiments on public datasets, Camelyon16 and TCGA-NSCLC, validate the efficacy of PAMT, highlighting consistent performance improvements across a variety of MIL benchmarks.

2 Method

Figure 1 presents the Prompt-guided Adaptive Model Transformation (PAMT) approach for Whole Slide Image Classification, which advances Whole Slide Image (WSI) classification through three methodical components: Representative Patch Sampling (RPS), Prototypical Visual Prompt (PVP), and Adaptive Model Transformation (AMT). Initially, an ImageNet pre-trained ResNet [7] extracts features, followed by RPS to identify representative patches through a pre-trained attention-based MIL. Subsequently, PVP assigns tailored visual prompts to these patches, enriching the input data. The AMT phase integrates adapter blocks into the feature extractor. Visual prompts and adapter blocks are fine-tuned in conjunction with the MIL classifier to ensure cohesive model adaptation. Details of each component are further elaborated in the following.

2.1 Representative Patch Sampling for End-to-End Training

The Representative Patch Sampling (RPS) technique addresses a critical challenge in WSI classification: the impracticality of processing an excessively high number of patches. Typically, conventional methods involve aggregating all patches extracted from a WSI into a single bag for MIL. However, a large portion of histological tissues may contain similar and non-informative content, making them redundant. Acknowledging that diagnostically significant patches often represent a minor fraction of the total, *e.g.*, less than 10% in Camelyon16 [3], RPS aims to identify and utilize these patches more efficiently. Through an attention-based MIL framework, patches are scored based on their relevance to the diagnostic outcome. We define this selection as:

$$\Phi(B_i) = \{x_{ij} | \alpha_{ij} \in \text{top-}K(\{\alpha_{ij}\}_{j=1}^{M_i})\}, \quad (1)$$

where α_{ij} denotes the attention score for j -th patch x_{ij} within bag B_i containing M_i patches. These scores are determined by an attention-based MIL classifier:

$$\alpha_{ij} = \frac{\exp\{\mathbf{w}^T (\tanh(\mathbf{V}_1 f(x_{ij})) \odot \text{sigmoid}(\mathbf{V}_2 f(x_{ij})))\}}{\sum_{j=1}^{M_i} \exp\{\mathbf{w}^T (\tanh(\mathbf{V}_1 f(x_{ij})) \odot \text{sigmoid}(\mathbf{V}_2 f(x_{ij})))\}}, \quad (2)$$

where \mathbf{w} , \mathbf{V}_1 , and \mathbf{V}_2 represent the learnable parameters within the MIL classifier, and the element-wise multiplication is denoted by \odot .

By concentrating on the top- K scoring patches, the RPS approach substantially reduces computational load and enables a more focused and effective model training pathway. This method enhances the model’s capacity to discriminate based on critical diagnostic features, resulting in an enriched set of patches that are truly representative of the pathological state of the WSI.

2.2 Prototypical Visual Prompt for Complex Data Distribution

Unlike natural images, WSIs exhibit significant intra- and inter-slide heterogeneity (*e.g.*, variations in tissue characteristics and staining techniques), which poses distinct challenges for WSI classification. To navigate this complexity, we introduce Prototypical Visual Prompt (PVP), which aims to enhance the representation of features aligned with the diverse pathological data distributions. Unlike the generic single visual prompt, PVP provides a set of tailored prompts to capture the unique diagnostic features of each patch.

Following the Representative Patch Sampling (RPS) process, a clustering algorithm (*e.g.*, k -means) groups the extracted features $\{f(x_{ij}) | x_{ij} \in \Phi(B_i), \forall i\}$ across all WSI bags, capturing the overarching pathological themes. This process identifies prototypical patterns within the data, resulting in cluster centroids $\{\mu_c\}_{c=1}^C$, which guide the assignment of visual prompts $\{p_c\}_{c=1}^C$ to corresponding patches. Finally, the prompted patches are aggregated to form the prompted bag $\Psi(B_i)$. This is mathematically represented as:

$$x'_{ij} = x_{ij} + p_{\epsilon_{ij}}, \quad (3)$$

$$\Psi(B_i) = \{x'_{ij} \mid x_{ij} \in \Phi(B_i)\}, \quad (4)$$

with the assignment ϵ_{ij} determined by the proximity to these centroids:

$$\epsilon_{ij} = \underset{c}{\operatorname{argmin}} \|f(x_{ij}) - \mu_c\|_2. \quad (5)$$

PVP are constructed as trainable padding prompts shown in Fig. 1, ensuring that each prompt is adaptable and specific to the cluster it represents. In this work, we set the number of clusters (C) and the padding size (S) to 4 and 10, respectively.[†] By infusing patches with PVP tailored to their cluster-specific features, the assembled bag enriches the model’s ability to discern the vast array of tissue characteristics inherent in WSIs, enhancing classification performance.

2.3 Adaptive Model Transformation with Transfer Learning

The transition from pre-trained natural image analysis to specialized pathological image classification presents a unique challenge. There is a need to retain the robust feature extraction capabilities honed on diverse datasets while ensuring the model is efficiently adapted to the specificities of pathological images. Considering the high volume and size of patches in WSIs yet the relatively lower number of slides compared to natural images, it is crucial to maintain the pre-training benefits while enhancing task-specific adaptability. To this end, we introduce Adaptive Model Transformation (AMT), a strategic approach for adaptively transforming the pre-trained model to the pathology domain.

AMT integrates adapter blocks positioned parallel to its foundational blocks. Here, AMT integrates three adapter blocks into the last layer of a pruned ResNet-50 [15]. The number and position of adapter blocks can be adaptively adjusted based on the specific task and dataset.[†] These adapters comprise a sequence of a global average pooling (GAP), followed by a two-layer multi-layer perceptron (MLP) and a sigmoid activation function, as depicted in Fig. 1. For an intermediate feature map \mathbf{f}_{i-1} as the input for the i -th ResNet block, an adapter block generates a domain-adaptive vector \mathbf{b}_i . This vector is then channel-wise multiplied with subsequent feature maps $g_i(\mathbf{f}_{i-1})$, facilitating a tailored feature adaptation, represented as:

$$\mathbf{b}_i = \operatorname{sigmoid}(\mathbf{W}_{i2} \operatorname{ReLU}(\mathbf{W}_{i1} \operatorname{GAP}(\mathbf{f}_{i-1}))), \quad (6)$$

$$\mathbf{f}_i = g_i(\mathbf{f}_{i-1}) \odot \mathbf{b}_i, \quad (7)$$

where $\operatorname{ReLU}(\cdot)$ denotes rectified linear unit, \mathbf{W}_{i1} and \mathbf{W}_{i2} are the learnable parameters to be fine-tuned, and the parameters of $g_i(\cdot)$ remain frozen during training. During the training process, only the parameters of visual prompts, adapter blocks, and the lightweight MIL classifier are updated in an end-to-end manner, while the original pre-trained feature extractor is frozen to retain the vast knowledge encoded in the pre-trained model.

[†] The ablation study of C and S can be found in the supplementary material.

[†] The ablation study of the position and quantity of adapter blocks can be found in the supplementary material.

Table 1. Results of comparative experiments on Camelyon16 and TCGA-NSCLC datasets. In the table, the best results are in bold. The mean and standard deviation is reported (mean_{std}) under 3 times’ experiments.

Method	Camelyon16			TCGA-NSCLC			
	AUC	F1	Acc	AUC	F1	Acc	
Baseline	Mean-pooling	0.590 _{0.018}	0.454 _{0.007}	0.677 _{0.011}	0.900 _{0.013}	0.834 _{0.011}	0.830 _{0.010}
	Max-pooling	0.854 _{0.028}	0.754 _{0.119}	0.826 _{0.037}	0.906 _{0.021}	0.843 _{0.025}	0.832 _{0.027}
	AB-MIL [9]	0.874 _{0.023}	0.798 _{0.013}	0.861 _{0.009}	0.928 _{0.018}	0.878 _{0.014}	0.874 _{0.016}
	CLAM-SB [15]	0.902 _{0.012}	0.827 _{0.021}	0.871 _{0.019}	0.925 _{0.023}	0.870 _{0.026}	0.874 _{0.022}
	DTFD-MIL [22]	0.910 _{0.011}	0.835 _{0.029}	0.884 _{0.027}	0.930 _{0.019}	0.887 _{0.017}	0.884 _{0.021}
PAMT	Mean-pooling	0.810 _{0.010}	0.714 _{0.013}	0.803 _{0.017}	0.925 _{0.011}	0.874 _{0.014}	0.871 _{0.010}
	Max-pooling	0.890 _{0.015}	0.777 _{0.016}	0.824 _{0.025}	0.926 _{0.013}	0.873 _{0.011}	0.870 _{0.013}
	AB-MIL [9]	0.921 _{0.011}	0.828 _{0.018}	0.866 _{0.008}	0.931 _{0.009}	0.884 _{0.007}	0.879 _{0.011}
	CLAM-SB [15]	0.924 _{0.009}	0.832 _{0.007}	0.881 _{0.006}	0.933 _{0.011}	0.891 _{0.006}	0.888 _{0.005}
	DTFD-MIL [22]	0.929 _{0.010}	0.859 _{0.007}	0.897 _{0.009}	0.942 _{0.008}	0.895 _{0.013}	0.893 _{0.014}

3 Experiments

3.1 Datasets

We evaluate our method on two public datasets: Camelyon16 [3] and TCGA-NSCLC [1]. Camelyon16 consists of 399 H&E WSI from breast cancer screening, with two classes: normal and tumor. We use the official 129 test set and split the official 270 training set into training and validation sets with a ratio of 9: 1. TCGA-NSCLC contains two subtypes of lung cancer: Lung Adenocarcinoma (LUAD) and Lung Squamous Cell Carcinoma (LUSC). We split the dataset into training, validation, and testing sets at the slide level, with a ratio of 65:10:25.

3.2 Implementation Details

The performance is measured by Accuracy (Acc), F1 score (F1), and Area Under the Curve (AUC). In the RPS process, we adopt the DTFD model [22] as the attention-based MIL classifier. The Adam optimizer [10] was employed for the adapter blocks and classifier with a learning rate and weight decay of 1e-4 over 100 epochs. Following [2], visual prompts were optimized using SGD [14] at a starting learning rate of 40 and decay according to a cosine schedule. These computations were facilitated by an NVIDIA GeForce RTX 3090 GPU.

3.3 Comparison with State-of-the-Art Methods

We compare our method with state-of-the-art methods on the Camelyon16 and TCGA-NSCLC datasets, including Mean-pooling, Max-pooling, AB-MIL [9], CLAM-SB [15], and DTFD-MIL [22]. Table 1 indicates a consistent enhancement in performance metrics when applying our PAMT approach compared to

Table 2. Ablation study of different tuning strategies using DTFD on the Camelyon16 dataset. ‘+’ denotes additional trained parameters beyond the common MIL classifier. ‘**Partial**’ trains the extractor’s last layer and MIL classifier. Averaged over three trials.

	Baseline	✓	✓	✓	✓	✓			
Method	RPS		✓	✓	✓	✓	Fully	Partial	BitFit
	PVP			✓		✓	-tuning	[18]	[21]
	AMT				✓	✓			
	AUC	0.910	0.916	0.922	0.924	0.929	0.891	0.911	0.912
Params(M)	0.789	+0	+0.118	+0.393	+0.511	+8.543	+7.098	+0.015	

the baseline methods. Notably, on the Camelyon16 dataset, our method significantly improved the performance of the baseline methods by 0.220, 0.036, 0.047, 0.022, and 0.019 in AUC, respectively. It is remarkable that our method significantly augmented the performance of both Mean and Max pooling strategies across both datasets, underscoring the enhanced quality of feature bags that enable these inherently less powerful MIL classifiers to achieve higher classification outcomes. The same trend is observed in the TCGA-NSCLC dataset.

3.4 Ablation Study

Effectiveness of each component. We conduct an ablation study to evaluate the effectiveness of each component in our method, including Representative Patch Sampling (RPS), Prototypical Visual Prompt (PVP), and Adaptive Model Transformation (AMT). As shown in Table 2, the baseline method DTFD achieves an AUC of 0.91 on the Camelyon16 dataset. After applying the RPS, the AUC increases to 0.914, indicating the effectiveness of representative patches with redundant information removal. Afterwards, the PVP and AMT further improve the AUC to 0.922 and 0.924, respectively. Integrating three techniques, the AUC reaches 0.929, demonstrating the combined advantages of different components in our method.

Comparison with other tuning strategies. In Table 2, we compare our method with other tuning strategies, including Fully-tuning, Partial-tuning [18], and BitFit [21]. All these strategies indicate an absence of significant improvement in model performance. Overfitting emerged as a concern with both the Fully and Partial tuning methods, due to the limited dataset size hindering generalization to novel data. BitFit may suffer from a lack of adaptability to the dataset’s intricacies. Conversely, our method exhibits a significant performance uplift without incurring significant parameter overhead.

Analysis under limited data. To further evaluate the robustness of our method, we explore more challenging scenarios with varying proportions of the training set within the TCGA-NSCLC dataset. As depicted in Fig. 2, our method

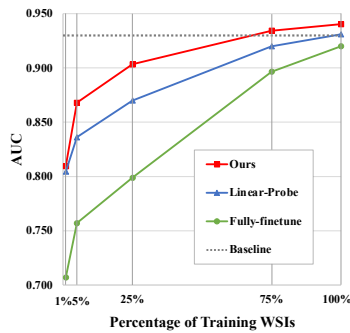


Fig. 2. Different training strategies with varying proportions of training WSIs using the DTFD model on TCGA-NSCLC dataset.

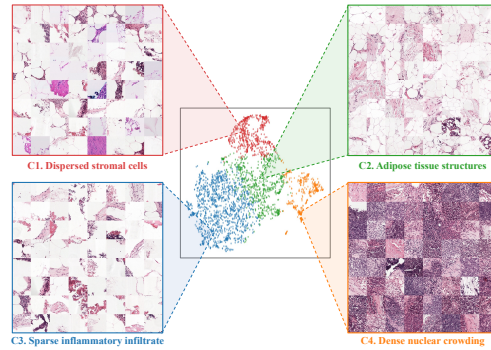


Fig. 3. Visualization of cluster centers for bag reprogramming. Four distinct clusters are showcased, representing varied histopathological features.

yields consistent superiority over the LP and Fully fine-tuning methods. Notably, employing merely 75% of the training data, our approach surpasses the baseline performance with the full dataset, underscoring the efficacy of our method in extracting and leveraging meaningful patterns from limited data and the potential for application in scenarios where data acquisition is challenging.

Visualization of cluster centers for PVP. In Fig. 3, we visualize the cluster centers obtained from the Prototypical Visual Prompt, which discerned four salient histopathological patterns matched with distinct padding prompts. Results demonstrate a spectrum of tissue characteristics, from sparse inflammatory infiltrates to areas of dense nuclear aggregation, which are likely to carry diagnostic relevance. This ablation study confirms the clustering process’s capacity to isolate and highlight significant histopathological features within the dataset.

4 Conclusion

In this study, we introduce *PAMT*, a Prompt-guided Adaptive Model Transformation approach for Whole Slide Image Classification. *PAMT* seamlessly incorporates three key components, namely Representative Patch Sampling (RPS), Prototypical Visual Prompt (PVP), and Adaptive Model Transformation (AMT), with the objective of revamping both the input data and the model. *PAMT* leverages visual prompts and adapter blocks while preserving the pre-trained backbone’s intrinsic knowledge, ensuring tailored adaption for pathology images. Comprehensive validation on two public datasets, Camelyon16 and TCGA-NSCLC, employing five distinct MIL classifiers, underscores that *PAMT* can considerably improve WSI classification, showing its effectiveness and efficiency. The future work will focus on the development of a more advanced visual prompt and adapter block in consideration of scalability, flexibility, and robustness.

References

1. The cancer genome atlas (tcga) dataset, <https://www.cancer.gov/tcga>
2. Bahng, H., Jahanian, A., Sankaranarayanan, S., Isola, P.: Exploring visual prompts for adapting large-scale models. arXiv preprint arXiv:2203.17274 (2022)
3. Bejnordi, B.E., Veta, M., Van Diest, P.J., Van Ginneken, B., Karssemeijer, N., Litjens, G., Van Der Laak, J.A., Hermsen, M., Manson, Q.F., Balkenhol, M., et al.: Diagnostic assessment of deep learning algorithms for detection of lymph node metastases in women with breast cancer. *Jama* **318**(22), 2199–2210 (2017)
4. Chen, T., Kornblith, S., Norouzi, M., Hinton, G.: A simple framework for contrastive learning of visual representations. In: International Conference on Machine Learning. pp. 1597–1607. PMLR (2020)
5. Cornish, T.C., Swapp, R.E., Kaplan, K.J.: Whole-slide imaging: routine pathologic diagnosis. *Advances in Anatomic Pathology* **19**(3), 152–159 (2012)
6. Hashimoto, N., Fukushima, D., Koga, R., Takagi, Y., Ko, K., Kohno, K., Nakaguro, M., Nakamura, S., Hontani, H., Takeuchi, I.: Multi-scale domain-adversarial multiple-instance cnn for cancer subtype classification with unannotated histopathological images. In: Proceedings of the IEEE/CVF Conference on Computer Vision and Pattern Recognition. pp. 3852–3861 (2020)
7. He, K., Zhang, X., Ren, S., Sun, J.: Deep residual learning for image recognition. In: Proceedings of the IEEE/CVF Conference on Computer Vision and Pattern Recognition. pp. 770–778 (2016)
8. Hou, L., Samaras, D., Kurc, T.M., Gao, Y., Davis, J.E., Saltz, J.H.: Patch-based convolutional neural network for whole slide tissue image classification. In: Proceedings of the IEEE/CVF Conference on Computer Vision and Pattern Recognition. pp. 2424–2433 (2016)
9. Ilse, M., Tomczak, J., Welling, M.: Attention-based deep multiple instance learning. In: International Conference on Machine Learning. pp. 2127–2136. PMLR (2018)
10. Kingma, D.P., Ba, J.L.: Adam: A method for stochastic optimization. In: International Conference on Learning Representations. pp. 1–15 (2014)
11. Lerousseau, M., Vakalopoulou, M., Classe, M., Adam, J., Battistella, E., Carré, A., Estienne, T., Henry, T., Deutsch, E., Paragios, N.: Weakly supervised multiple instance learning histopathological tumor segmentation. In: Medical Image Computing and Computer Assisted Intervention–MICCAI 2020: 23rd International Conference, Lima, Peru, October 4–8, 2020, Proceedings, Part V 23. pp. 470–479. Springer (2020)
12. Li, B., Li, Y., Eliceiri, K.W.: Dual-stream multiple instance learning network for whole slide image classification with self-supervised contrastive learning. In: Proceedings of the IEEE/CVF Conference on Computer Vision and Pattern Recognition. pp. 14318–14328 (2021)
13. Li, S., Liu, Y., Sui, X., Chen, C., Tjio, G., Ting, D.S.W., Goh, R.S.M.: Multi-instance multi-scale cnn for medical image classification. In: Medical Image Computing and Computer Assisted Intervention–MICCAI 2019: 22nd International Conference, Shenzhen, China, October 13–17, 2019, Proceedings, Part IV 22. pp. 531–539. Springer (2019)
14. Loshchilov, I., Hutter, F.: SGDR: Stochastic gradient descent with warm restarts. In: International Conference on Learning Representations (2016)
15. Lu, M.Y., Williamson, D.F., Chen, T.Y., Chen, R.J., Barbieri, M., Mahmood, F.: Data-efficient and weakly supervised computational pathology on whole-slide images. *Nature Biomedical Engineering* **5**(6), 555–570 (2021)

16. Pantanowitz, L., Valenstein, P.N., Evans, A.J., Kaplan, K.J., Pfeifer, J.D., Wilbur, D.C., Collins, L.C., Colgan, T.J.: Review of the current state of whole slide imaging in pathology. *Journal of Pathology Informatics* **2**(1), 36 (2011)
17. Pinckaers, H., Van Ginneken, B., Litjens, G.: Streaming convolutional neural networks for end-to-end learning with multi-megapixel images. *IEEE Transactions on Pattern Analysis and Machine Intelligence* **44**(3), 1581–1590 (2020)
18. Shen, Z., Liu, Z., Qin, J., Savvides, M., Cheng, K.T.: Partial is better than all: revisiting fine-tuning strategy for few-shot learning. In: *Proceedings of the AAAI Conference on Artificial Intelligence*. vol. 35, pp. 9594–9602 (2021)
19. Srinidhi, C.L., Ciga, O., Martel, A.L.: Deep neural network models for computational histopathology: A survey. *Medical Image Analysis* **67**, 101813 (2021)
20. Stacke, K., Eilertsen, G., Unger, J., Lundström, C.: Measuring domain shift for deep learning in histopathology. *IEEE Journal of Biomedical and Health Informatics* **25**(2), 325–336 (2020)
21. Zaken, E.B., Goldberg, Y., Ravfogel, S.: Bitfit: Simple parameter-efficient fine-tuning for transformer-based masked language-models. In: *Proceedings of the 60th Annual Meeting of the Association for Computational Linguistics*. pp. 1–9 (2022)
22. Zhang, H., Meng, Y., Zhao, Y., Qiao, Y., Yang, X., Coupland, S.E., Zheng, Y.: DTFD-MIL: Double-tier feature distillation multiple instance learning for histopathology whole slide image classification. In: *Proceedings of the IEEE/CVF Conference on Computer Vision and Pattern Recognition*. pp. 18802–18812 (2022)
23. Zhang, J., Kapse, S., Ma, K., Prasanna, P., Saltz, J., Vakalopoulou, M., Samaras, D.: Prompt-MIL: Boosting multi-instance learning schemes via task-specific prompt tuning. *arXiv preprint arXiv:2303.12214* (2023)
24. Zhu, Y., Shen, Z., Zhao, Z., Wang, S., Wang, X., Zhao, X., Shen, D., Wang, Q.: Melo: Low-rank adaptation is better than fine-tuning for medical image diagnosis. *arXiv preprint arXiv:2311.08236* (2023)